ChemPubSoc Europe

DOI: 10.1002/chem.201504899

CHEMISTRY A European Journal Full Paper

Chirality |*Hot Paper*|

Inherently Chiral Spider-Like Oligothiophenes

Francesco Sannicolò,[a] Patrizia R. Mussini,*[a] Tiziana Benincori,*[b] Rocco Martinazzo,*[a] Serena Arnaboldi,[a] Giulio Appoloni,[b] Monica Panigati,[a] Elsa Quartapelle Procopio,[a] Valentina Marino,[a] Roberto Cirilli,[c] Simone Casolo,[a] Wlodzimierz Kutner,[d] Krzysztof Noworyta,[d] Agnieszka Pietrzyk-Le,[d] Zofia Iskierko,[d] and Katarzyna Bartold[d]

Abstract: The racemate of an inherently chiral "spider-like" octathiophene monomer **T8$_3$**, in which chirality is generated by torsion in its backbone, was synthesized. The racemate was resolved into configurationally stable antipodes by HPLC on a chiral stationary phase. Electrooxidation of the enantiomers resulted in materials displaying high enantiorecognition ability towards the antipodes of some chiral probes. Moreover, the **T8$_3$** racemate demonstrated great aptitude to stimulate formation of 3D rigid architectures if used as a cross-linking monomer for molecular imprinting. This feature was exploited to devise a molecularly imprinted polymer-based chemosensor selective for a thymine–adenine oligonucleotide.

Introduction

We recently devised an innovative strategy for the design of chiral functional materials based on the concept of the "inherent chirality": it implies that the same molecular moieties constituting the stereogenic elements responsible for chirality also provide the material with its specific properties.[1]

We have applied this approach to prepare chiral D_n symmetric macrocyclic oligothiophenes by chemical or electrochemical oxidation of monomers (*R*)-**1** and (*S*)-**1**, (Scheme 1),[2] where chirality is not introduced by attaching chiral pendants to the electroactive backbone, according to the most popular strategy,[3] envisaged by Roncali nearly thirty years ago,[4] but it is inherent to it. The conjugated oligothiophene system responsible for the optical and electrochemical properties also constitutes the atropisomeric scaffold responsible for chirality. We found that these materials exhibit impressive chiroptical properties correlated to the electrochemical ones and unprecedented ability to pronouncedly separate voltammetry peaks of enantiomers of quite different chiral probes.[5]

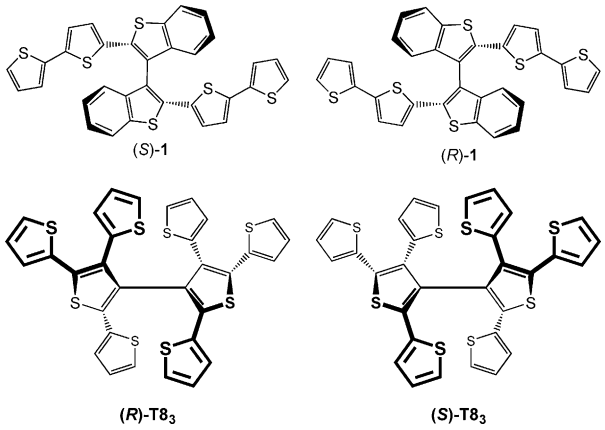

Scheme 1. Structural formulas of the inherently chiral monomers (*R*)- and (*S*)-**1** and the spider-like oligothiophenes (*R*)- and (*S*)-**T8$_3$**.

In this paper we report the results of a research aiming to apply the inherent chirality concept to the "spider-like" oligothiophenes, a class of branched all-thiophene molecules we investigated a few years ago, characterized by an inner core, from thiophene to pentathiophene (the trunk of the spider), persubstituted with 2-thienyl[6] or 2-(5,2′-bithienyl)[7] units (the legs).

Multi-branched oligothiophene molecules have attracted considerable attention on account of their 3D conjugated architectures endowed with isotropic charge transport and optical properties, coupled with high chemical stability and remarkable solubility in organic non-polar solvents.[8] We considered it to be of interest to couple these properties with

[a] *Prof. F. Sannicolò, Prof. P. R. Mussini, Prof. R. Martinazzo, Dr. S. Arnaboldi, Dr. M. Panigati, Dr. E. Quartapelle Procopio, V. Marino, Dr. S. Casolo*
Dipartimento di Chimica Università degli Studi di Milano
Via Golgi 19, 20133 Milano (Italy)
E-mail: patrizia.mussini@unimi.it
rocco.martinazzo@unimi.it

[b] *Prof. T. Benincori, G. Appoloni*
Dipartimento di Scienza e Alta Tecnologia
Università degli Studi dell'Insubria Via Valleggio 11, 22100 Como (Italy)
E-mail: tiziana.benincori@uninsubria.it

[c] *Dr. R. Cirilli*
Dipartimento del Farmaco
Istituto Superiore di Sanità Viale Regina Elena 299, 00161 Roma (Italy)

[d] *Prof. W. Kutner, Dr. K. Noworyta, Dr. A. Pietrzyk-Le, Z. Iskierko, K. Bartold*
Institute of Physical Chemistry Polish Academy of Sciences
Kasprzaka 44/52, 01-224 Warsaw (Poland)

Supporting information and ORCID number(s) for the author(s) of this article are available on the WWW under
http://dx.doi.org/10.1002/chem.201504899.

chirality and, in this light, we synthesized the C_2 symmetric 2,2′,4,4′,5,5′-hexa(2-thienyl)-3,3′-bithiophene (**T8$_3$**).

We focused our attention not only on the enantiorecognition ability of the enantiopure antipodes of the **T8$_3$**, but we also exploited its racemate to synthesize a co-polymer molecularly imprinted with the TATAAA (T-thymine, A-adenine) oligonucleotide, employed as a recognition unit of the extended-gate field-effect transistor (EG-FET) chemosensor.

Results and Discussion

T8$_3$ was easily prepared in acceptable yields by Stille reaction of the hexabromo-3,3′-bithiophene with 2-tributylstannylthiophene.

T8$_3$ structure differs from the "swivel cruciform" α-terthiophene dimer (**BT3**), a *p*-type semiconductor investigated by Scherf, for the presence of the 2-thienyl units in position *ortho* to the bond containing the stereogenic axis responsible for the atropisomerism.[9] They also formally result from doubling the 5′-(2-thienyl)-2,2′,3′,2″-terthiophene (**4T**), a monomer widely used by Ludwigs for preparing hyperbranched polythiophenes by electrochemical or chemical oxidation.[8e–g] This monomer is also the constitutional isomer of the **T′8$_4$**, a member of the class of the spider-like oligothiophenes cited above (Scheme 2).[6]

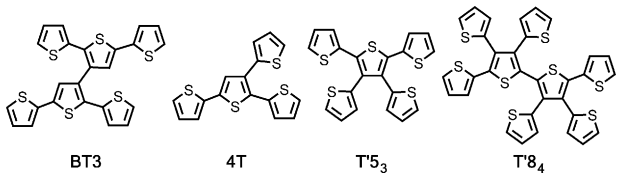

Scheme 2. Structural formulas of oligothiophenes structurally related to **T8$_3$**.

DFT calculations provided interesting information on the conformational properties of **T8$_3$**, on the configurational stability of the enantiomers, and on the π-electron distribution on the different thiophene rings. First of all, the calculated racemization energy barrier for the enantiomers is very high (178.74 kJ mol^{-1}), thereby granting their configurational stability.

The equilibrium geometry of the most stable conformer exhibits two homotopic α-terthiophene units orthogonal to each other (dihedral angle Cα-Cβ-Cβ′-Cα′ = −97.3°), with the three rings substantially coplanar and the 2-thienyl groups in β-position nearly perpendicular to them (dihedral angle Cα-Cβ-Cα″-Cβ″ = 109.5°). Similar structures were found for different conformers when turning each of the thienyl groups around their interannular C–C links. They lie slightly higher in energy than the example shown in Figure 1 (≈0.25–1.4 kJ mol^{-1} depending on the specific thienyl unit considered) and are easily accessible under normal conditions.

DFT calculations revealed that both the HOMO and the HOMO-1 orbitals have sizable amplitude on the α-terthiophene moieties and modest weight on the β-connected units, a result which is further confirmed by the distribution of the spin-density of both the radical cation and radical anion.This result suggests that the preferred electrooxidation-electrooligomerization sites in **T8$_3$** are the four α-positions of the two homotopic α-conjugated fragments. Considering that the terminal α-positions of each terthiophene unit are constitutionally heterotopic and the architecture of the molecule is tridimensional and rigid, we expected a very stiff cross-linked network of interconnected heterotopic thiophene units when **T8$_3$** was subjected to oxidative electrooligomerization.

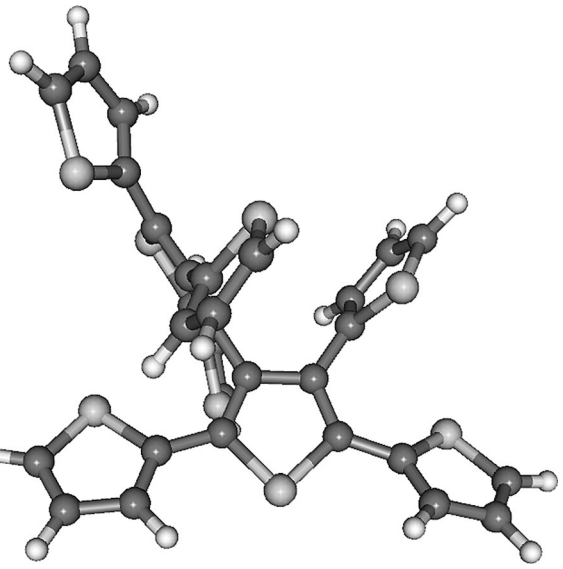

Figure 1. Calculated preferred conformation for (*R*)-**T8$_3$**.

The above structural characteristics are confirmed by the electronic spectrum showing absorption λ_{max} at 371 nm in toluene solution ($\varepsilon = 27\,000\ M^{-1}\,cm^{-1}$, Figure 2), attributable to the spin-allowed π–π* transition. This band is redshifted by 10 nm compared to that of the analogous **BT3** ($\lambda_{max} = 361$ nm)[10] and redshifted by 16 nm compared to that of α-terthiophene ($\lambda_{max} = 355$ nm, $\varepsilon = 19\,000\ M^{-1}\,cm^{-1}$) in chloroform solution.[11] Noticeably, the same redshift of about 10 nm is observed for **T′5$_3$** ($\lambda_{max} = 361$ nm)[6] (Scheme 2), formally resulting from the addition of a second thiophene ring in the β position of the central ring of the α-terthiophene moiety of **4T** ($\lambda_{max} = 352$ nm).[12] This behaviour suggests a weak electronic interaction through the α–β connection.

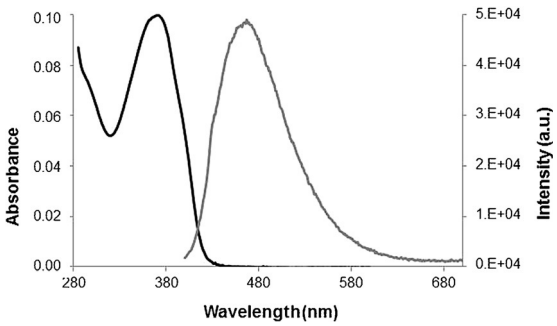

Figure 2. The UV/Vis (dark line) and emission (light line) spectra of **T8$_3$** in aerated toluene solution at 298 K.

The same absorption maximum observed for **T8$_3$** is shown also by **T′8$_4$**, the isomeric spider-like oligothiophene (λ_{max} = 370 nm).[6] This means that the decrease in efficiency of the α–α conjugation observed in the case of **T′8$_4$** has the same influence on the optical properties of the β–β connection in **T8$_3$**.

The value of the extinction coefficient determined for **T8$_3$**, which is higher than that expected for a single terthiophene chain, but lower than that expected for two chains, can be ascribed to the branched structure of the molecule.

Upon optical excitation with UV light (λ_{ex} = 380 nm), **T8$_3$** displays a broad and featureless emission band at 467 nm in the toluene aerated solution (Figure 2), with the photoluminescence quantum yield ϕ = 0.012. The emission maximum lies between those observed for the analogous **BT3** (λ_{em} = 478 nm) and the α-quarterthiophene (λ_{em} = 453 nm, with a shoulder at 478 nm, in dry THF, ϕ = 0.24).[13] However, as in the case of **BT3**, the emission band is broad and no vibrational structure is observed, indicating a reduced planarization in the excited state. The higher conformational reorganization, required in the electronic excitation for **T8$_3$** and **BT3** with respect to the linear α-terthiophene or α-quaterthiophene, accounts for the higher Stokes shift observed (≈100 nm for **T8$_3$** and **BT3** vs. 50–60 nm for the linear oligothiophenes). The very low value of the photoluminescence quantum yield is connected to the geometry of the excited state, because non-radiative deactivation pathways, favored by torsional vibration motions induced by the presence of the thiophenes in β positions, are easily accessible.

The resolution of racemic (±)-**T8$_3$** by HPLC on a chiral stationary phase presents some difficulties related to the low resolution factor (Figure 3 a), so that only minute amounts of enantiopure antipodes could be obtained.

The configuration assignment to the enantiomers was performed by comparison of the experimental CD curves (Figure 3 b) with that calculated for the (*S*)-antipode. The latter corresponded to the first eluted dextrorotatory enantiomer (Figure SI3 in the Supporting Information).

The redox properties of **T8$_3$** have been studied by cyclic voltammetry (CV), in dichloromethane and acetonitrile (ACN), both with 0.1 M (TBA)PF_6 supporting electrolyte, and in the butylmethylimidazolium hexafluophosphate, (BMIM)PF_6, ionic liquid. A comparison of CV features in the three media on glassy carbon (GC) electrode, plotted versus the intersolvental $Fc^+|Fc$ reference redox couple, is shown in Figure 4 (Au and Pt were also tested, with similar results, see the Supporting Information SI5).

In ACN and (BMIM)PF_6 both oxidation and reduction peaks can be observed, affording to estimate HOMO–LUMO gaps for the molecule, 2.93 and 2.89 eV respectively, only slightly lower than that of linear α-terthiophene (3.1 eV).[14] This is in agreement with the **T8$_3$** structure consisting of two α-terthiophene moieties, with low or null conjugation on account of the very high torsional angle (in branched oligothiophenes electronic properties are essentially determined by the longest conjugated chain).[6,7,8c]

As in the case of the inherently chiral monomers **1**,[1] on the oxidation side, a two-peak system is clearly observed in the two conventional media, and perceived in the ionic liquid too,

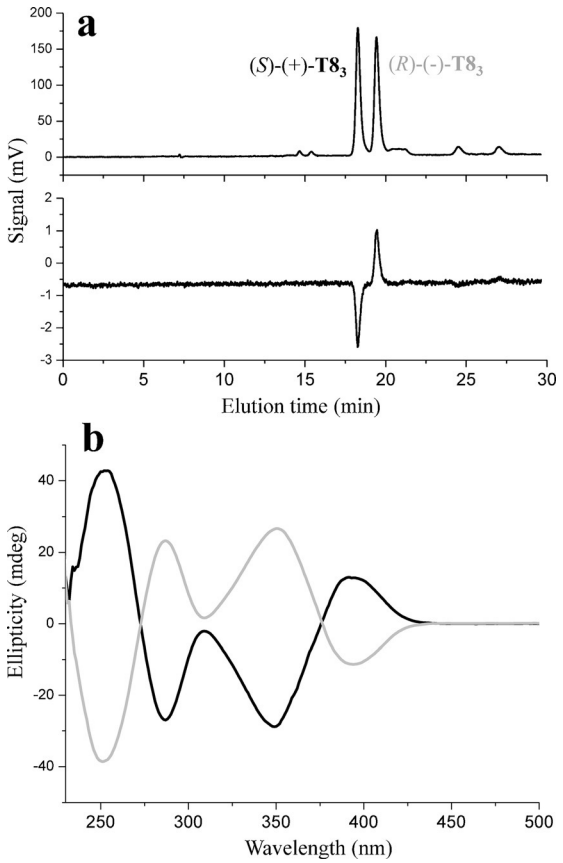

Figure 3. a) HPLC resolution of (±)-**T8$_3$**. CSP: Chiralpak IB-3, 250×4.6 mm I.D.+Chiralpak IB-3, 250×4.6 mm I.D.; eluent: *n*-hexane/dichloromethane/ethanol 100/5/0.2; flow-rate: 1.0 mL min^{-1}; temperature: 25 °C; detection: UV (top) and CD (bottom) at 350 nm. b) CD spectra ($CHCl_3$) of (+)-**T8$_3$** (black) and (−)-**T8$_3$** (grey).

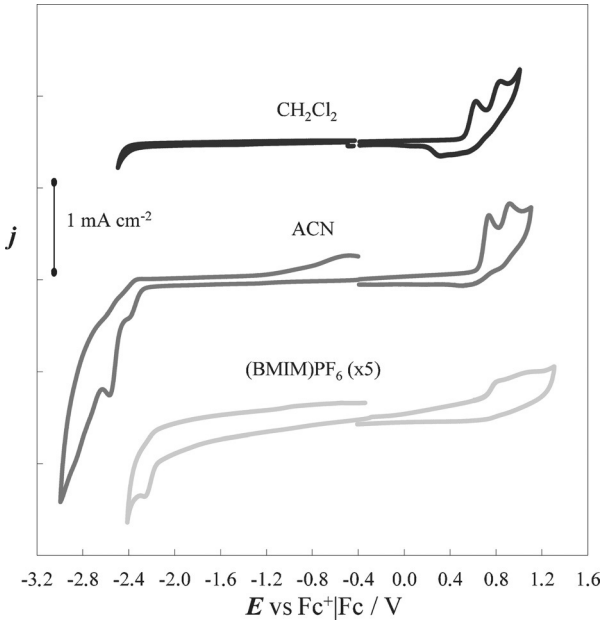

Figure 4. CV patterns at 0.2 V s^{-1} for 0.0005 M monomer **T8$_3$** on the GC electrode (0.031 cm^2) in different media. Top curve: dichloromethane + 0.1 M (TBA)PF_6; middle curve: acetonitrile + 0.1 M (TBA)PF_6; bottom curve: (BMIM)PF_6 ionic liquid (×5).

in spite of poorer signal resolution. Again, such patterns could account for two equivalent redox centers reciprocally interacting in space, corresponding to the two identical moieties. In fact, on one hand, the second oxidation peak could hardly be assigned to the oxidation of a product of the first oxidation, because the current ratio of the two peaks appears ~1 and nearly independent of the scan rate (Figure SI6 in the Supporting Information). On the other hand, te second oxidation on a terthiophene chain occurs at a potential of ≈1.0 V higher than that of the first oxidation (Table 1), so each oxidation process should take place on a different moiety. This assumption is also supported by the potential difference between the two peaks, which is larger in CH_2Cl_2 with respect to ACN (0.23 V vs. 0.19 V), possibly accounting for higher interaction between the two charges, on account of the lower solvent screening effect.

Both oxidative peaks are only moderately shifted to more positive potentials as the scan rate increases (Figure SI6 in the Supporting Information), pointing to rather facile electron transfers. On the other hand, the absence of symmetrical return peaks and the presence of irregular negative peaks at less positive potentials point to the electron transfer products undergoing a chemical reaction, in particular, coupling of radical cations in α-terminal positions. Actually, no less than four α-terminal positions (two identical pairs of constitutionally heterotopic sites with nearly equivalent properties) are available for oligomerization on the **T8$_3$** monomer (instead of the two homotopic ones of identical properties available for **1**), although, following the above considerations, it is improbable that more than one position per terthiophene chain would be activated at the same time as the radical cation at the first two oxidation potentials.

Electroactive films regularly grow on the electrode by potential cycling (Figure 5 and Figure SI7 in the Supporting Information). Slow growth, affording very regular films, is observed if the scan is reversed at a potential in between the first and the second oxidation peak; on the contrary, much faster growth is observed when the scan is reversed after the second oxidation peak.

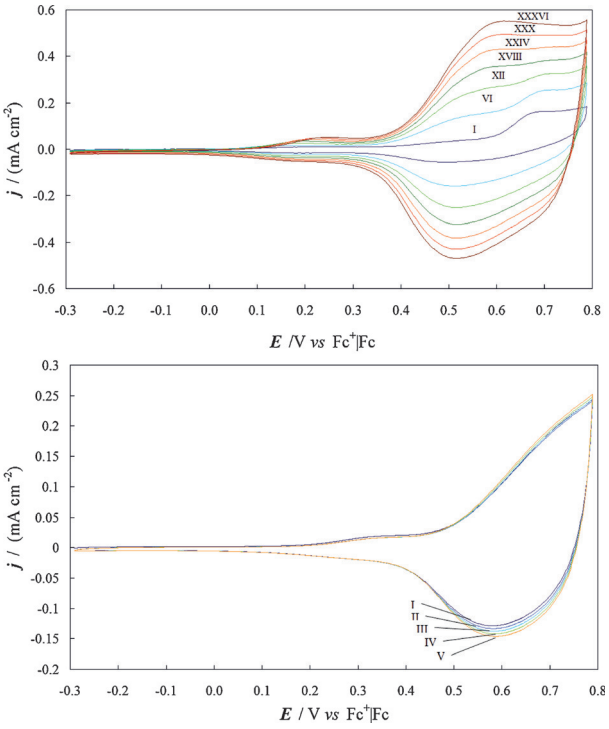

Figure 5. Multicycle curves of potentiodynamic electropolymerization (36 cycles, 0.05 V s^{-1} scan rate) of 0.01 M **T8$_3$** (above) and film stability (below) in (BMIM)PF_6 ionic liquid on Au SPE (geometric surface ≈0.11 cm^2). Scan numbers are indicated with Roman numerals.

Table 1. Electrochemical data of some oligothiophenes and their electrooligomerization films, with corresponding HOMO and LUMO energies and gaps

	E_{1c} vs. $Fc\|Fc^+$ [V]	$E_{p,a\,I}$ vs. $Fc\|Fc^+$ [V]	$E_{p,a\,II}$ vs. $Fc\|Fc^+$ [V]	E_{LUMO} [eV]	E_{HOMO} [eV]	E_G [eV]
MONOMERS						
α-**T$_3$**[a]	−2.50[b]	0.58[b]	1.53[b]	−2.30	−5.38	3.08
T′8$_{4\alpha\alpha\alpha}$[c]	−2.46[d]	0.63[d]	0.84[d]	−2.34	−5.43	2.88
T8$_{3\beta\beta}$[e]	n.d.	0.62[d]	0.85[d]	n.d.	−5.42	n.d.
T8$_{3\beta\beta}$[f]	−2.38[d]	0.74[d]	0.93[d]	−2.42	−5.54	3.12
T8$_{3\beta\beta}$[g]	−2.26[d]	0.81[d]	1.06[d]	−2.54	−5.61	3.07
OLIGOMER FILMS						
T′8$_{4\alpha\alpha\alpha}$[c]	−1.40[h]	0.20[h]		−3.40	−5.00	1.60
T8$_{3\beta\beta}$[e]	−1.33[h]	0.20[h]		−3.47	−5.00	1.53
T8$_{3\beta\beta}$[f]	−1.84[h]	0.38[h]		−2.96	−5.18	2.22
T8$_{3\beta\beta}$[g]	n.d.	0.43[h]		n.d.	−5.23	n.d.

[a] Ref. [14]. [b] Formal potentials $E^{\circ\prime}$. [c] CH_2Cl_2 + 0.1 M TBAP, GC electrode (Ref. [6]; $E_{p,a\,II}$ unpublished data). [d] Peak potentials E_p. [e] CH_2Cl_2 + 0.1 M $(TBA)PF_6$, GC electrode. [f] ACN + 0.1 M $(TBA)PF_6$, GC electrode. [g] $(BMIM)PF_6$, GC electrode. [h] Onset potentials E_{onset}. n.d. = not determined.

Film growth occurs on all supports and in all solvents. Cycling around the first oxidation peak (Figure SI7 in the Supporting Information), the deposition rate follows the sequence ACN > CH_2Cl_2 > IL. This sequence could arise from a combination of factors. The growing oligomers could be more soluble in the more apolar solvent; moreover, in the more polar solvent, reduced Coulombic repulsion of radical cations should facilitate coupling;[15] besides, a polar solvent typically increases reaction rate if charged species are formed.[16] In the IL case, however, the extremely high viscosity should prevail on the former effects. Remarkably, including the second oxidation peak, the scan rate greatly increases (the effect is particularly conspicuous in the CH_2Cl_2 case) and the oligomerization pattern changes remarkably (an example is provided in Figure SI7b in the Supporting Information), a feature which could be the object of further investigation.

All the electrodeposited films are stable upon subsequent oxidative potential cycling in a monomer-free solution (Figure 5). Moreover, neat charge-trapping effects are observed in the traditional media (Figure SI9 in the Supporting Information).

It is interesting to compare the electrochemical properties of **T8$_3$** and its films, deposited by electrooxidation, with those ex-

hibited by constitutional isomer **T′8$_4$** and its films (Table 1). Evidently, the electrochemical data are nearly identical, even though the α-conjugated thiophene sequence for the latter compound is longer. However, as already discussed, the torsion around the bond connecting the central thiophene units halves the α-tetrathiophene chain of **T′8$_4$** into two bithiophene moieties with small reciprocal conjugation, whereas such distortion does not decrease the longest α-terthiophene sequence in **T8$_3$**. The combination of these effects smoothes the differences in the electronic properties of these monomers, as also confirmed by the UV/Vis absorption spectra (Figure 2).

The enantiorecognition ability of enantiopure oligo-**T8$_3$** films was tested with two structurally different probes and two different protocols, previously developed for the oligo-**1** films.[1,5]

The first test was performed with (*R*)- and (*S*)-*N*,*N*-dimethyl-1-ferrocenylethylamine probes ((*R*)-**2** and (*S*)-**2**), both enantiopure and as the racemate. They have been chosen for electrochemical reversibility and commercial availability. (*R*)- or (*S*)-oligo-**T8$_3$** films electrodeposited on Au screen-printed electrodes (SPE) from a drop of monomer solution in (BMIM)PF_6 ionic liquid were used (36 oligomerization potential cycles, **T8$_3$** 12 mM, scan rate = 50 mV s^{-1}).

An impressive and specular discrimination was obtained for the enantiopure probes on the enantiopure oligo-**T8$_3$** electrode surfaces, with a peak separation of ≈250 mV (Figure 6), that is, even larger than that observed in the case of oligo-**1** with the same probes.[1]

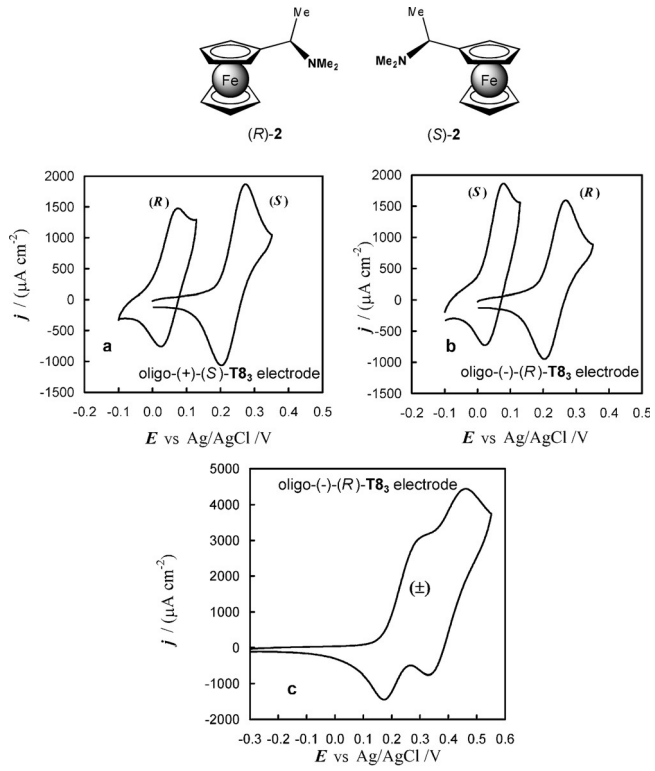

Figure 6. Enantiorecognition CV tests with (*R*)-**2** and (*S*)-**2** chiral redox probes (8 mM); a) oligo-(+)-(*S*)-**T8$_3$** film coated electrode; b) oligo-(−)-(*R*)-**T8$_3$** film coated electrode; c) with the (±)-**2** racemic redox probe on the oligo-(−)-(*R*)-**T8$_3$** film coated electrode. Scan rate: 50 mV s^{-1}.

Moreover, enantioselectivity was observed with the racemic probe even though, in this case, peak separation was significantly lower (≈150 mV), unlike the oligo-**1** modified SPEs, for which peak separation was higher in the case of the racemate. Furthermore, for the racemate of the probe, the peak potentials are remarkably shifted to more positive potentials with respect to those observed for the pure enantiomers of the probe. This suggests the occurrence of some reciprocal interaction of the two antipodes in the sensing process within the chiral film (Figure 6). A similar three-actor effect was previously observed for the oligo-**1** case, even though it was far less pronounced.

The second test was performed on enantiopure L- and D-DOPA (0.016 M) in 0.05 M HCl, using (*R*)-oligo-**T8$_3$** film deposited by electrooxidation on the Au SPE.

Similarly, a neat enantiodiscrimination was achieved, although with a less spectacular peak separation (60–70 mV) than in the former case (but similar to the ≈90 mV separation achieved with the electrodes modified with oligo-**1** films) (Figure 7).[5]

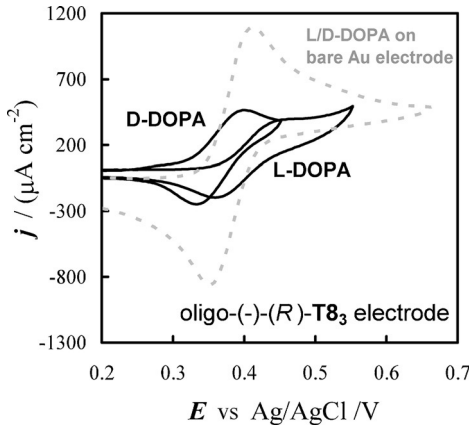

Figure 7. Enantiorecognition CV tests with D-DOPA and L-DOPA chiral redox probes (0.016 M) on the oligo-(−)-(*R*)-**T8$_3$** film coated electrode. Scan rate: 50 mV s^{-1}.

Based on the peculiar structural features of **T8$_3$** described above, we envisaged application of this octathiophene as an efficient cross-linking monomer for molecular imprinting in polymers.[17] If used as such a monomer, **T8$_3$** should promote formation of a polymer of a structure very advantageous for molecularly imprinted polymers (MIPs). In the MIP synthesis, a cross-linking and functional monomer is co-polymerized in the presence of a selected template, which is subsequently removed from the resulting MIP, leaving empty molecularly imprinted cavities capable of recognizing the original imprinter.[18] Electrochemical co-polymerization of **T8$_3$** would result in an MIP with a structure facilitating analyte permeation through the MIP matrix on the one hand and stabilizing tailored molecular cavities on the other.[19]

To test the usefulness of this **T8$_3$** application, we used this oligothiophene as a cross-linking monomer for deposition by electropolymerization of an MIP imprinted with the 5′-TATAAA-3′ oligonucleotide, that is, a TATA box promoter (Figure 8). In-

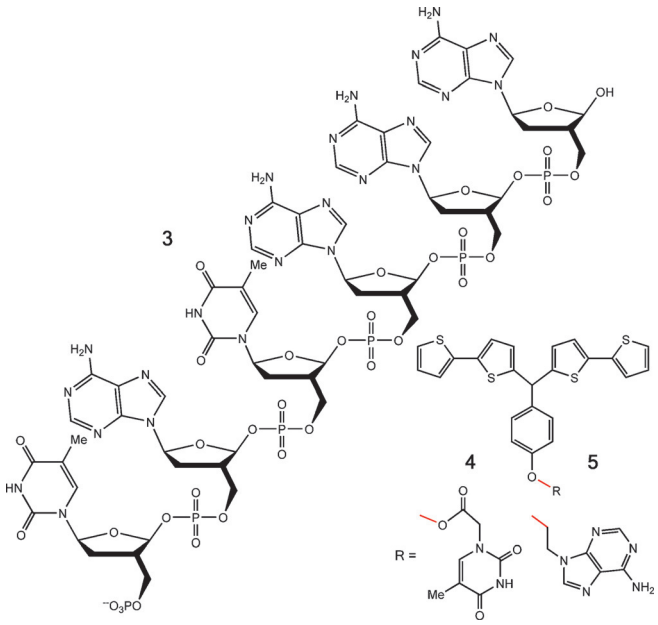

Figure 8. Structural formulas of the templating molecule, 5′-TATAAA-3′ **3**, as well as functional co-monomers **4** and **5**.

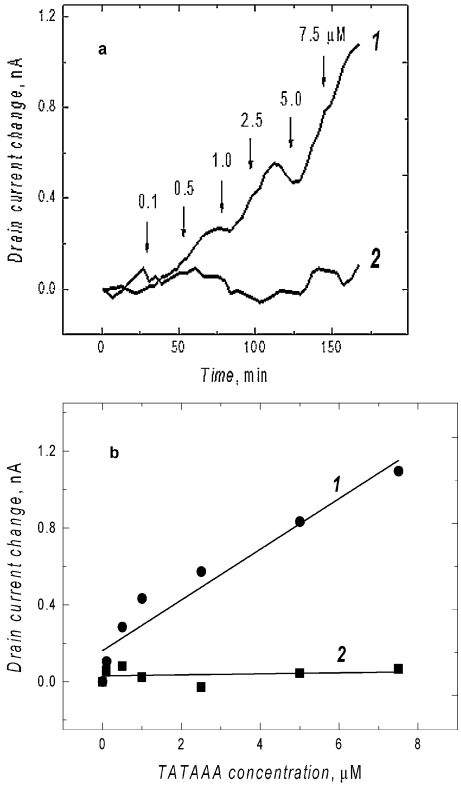

Figure 9. a) The background-corrected drain current changes with time for the EG-FET chemosensor with the gate area of the Au-glass slide coated with (*1*) the MIP-TATAAA thin film and (*2*) the NIP film. Extended-gate surface area: 21 mm^2; gate voltage: 1.50 V. b) The TATAAA calibration plots for the EG-FET chemosensor with the recognition unit of (*1*) the TATAAA-extracted MIP film and (*2*) the NIP film.

formation contained within the TATAAA is critical for proper initiation of transcription in eukaryotes. Sensitive and selective nucleotide determination is important in several fields[20] including clinical diagnostics,[21] environmental monitoring,[22] detection of biological threats,[23] and food safety.[24] The devised MIP was subsequently used as a recognition unit of the EG-FET selective TATAAA chemosensor.

For the TATAAA imprinting, we used bis[2-(5,2′-bithienyl)]methane functional monomers **4** and **5**, bearing thymine and adenine pendant, respectively, to form in solution a pre-polymerization complex with **3** through Watson–Crick type hydrogen bonds (Figure 8).

The EG-FET based technique is an interesting extension of the field-effect transistor transduction method developed in 1970.[25] As the conventional FET transductor, the EG-FET is based on the measurement of changes of the source-drain current at constant gate voltage when it is modulated by the gate voltage changes incurred by sorption of charged species within the gate region of the transistor. This effect can readily be used as a transduction method in the chemosensor.[26] In the EG-FET construction, the gate region can be electrically "extended" to outside metallic electrode, which greatly facilitates the modification of the sensor surface. This technique has already been successfully used for fabrication of various sensors,[27] including MIP-based ones.[28,29]

For TATAAA determination with the EG-FET chemosensor, either the MIP-TATAAA or the NIP-coated Au-glass electrode and the Pt grid as pseudo-reference electrode were immersed in a test aqueous solution and connected to the gate of the MOSFET. Gate voltage was set to 1.5 V and source-drain current changes were monitored. Increasing amounts of TATAAA analyte aqueous solution were consecutively added to the test aqueous solution under batch conditions. The EG-FET responses of the TATAAA chemosensors with either the MIP or NIP recognition unit are presented in Figure 9a. After each addition of the TATAAA analyte solution, the source-drain current increased for both the MIP and NIP film-coated EG-FET gate. However, changes observed for the MIP were much more significant than those for the NIP-coated electrode.

From these curves, calibration plots for the TATAAA-extracted MIP and the NIP film coating the EG-FET were constructed (Figure 9b). For the former, the linear dynamic concentration range extended from 0.1 to 7.5 μM TATAAA (Curve *1* in Figure 9b). This behaviour obeys the linear regression equation: I_d/nA = [16.2 ($\pm$5.7) $\times 10^{-5}$/nA + 13.2($\pm$1.6)] $\times 10^{-5}$ nA μM^{-1}. The sensitivity and correlation coefficient were (13.2 $\pm$ 1.6) μM^{-1} and 0.96, respectively. Of note, the NIP-coated sensor response to TATAAA was much lower, indicating effective formation of selective cavities in the MIP film.[29]

Conclusion

The results obtained, combining the peculiar properties of the all-thiophene branched materials with the enantiorecognition ability deriving from chirality, are very promising. The first "inherently chiral" spider-like oligothiophene **T8$_3$**, in which the electroactive backbone coincides with the stereogenic axis, is synthetically accessible in three steps from inexpensive and

commercially available compounds. Its electronic properties have been studied by means of spectroscopic and electrochemical investigations, as well as of theorethical calculations, and compared with other popular achiral, linear, and branched multi-thiophene systems.

The electrooxidation of the enantiomers produces stable enantiopure films displaying remarkable enantiorecognition ability towards the enantiomers of some chiral redox probes, clearly differentiating their oxidation potentials.

Finally, **T8$_3$**, when used as the monomer or co-monomer in electrooligomerization processes, is able to weave rigid cross-linked 3D frameworks, sufficiently porous for analyte penetration into the polymer matrix. An MIP film for the selective determination of an artificial nature-mimicking a single-stranded oligonucleotide was successfully developed with potential applications in clinical analysis.

Experimental Section

Organic synthesis

Melting points were measured by a Büchi B-540 instrument. NMR spectra were recorded on a Bruker AV 300 spectrometer. Chemical shifts are given in ppm (δ, dd = double doublet). Mass spectra were recorded on Bruker Daltonics high-resolution FT-ICR model APEXTM II (4.7 T Magnex cryomagnet supplied with ESI source).

Hexabromo-3,3′-bithiophene:[30] Br_2 (5.0 mL; 96 mmol) was dropped into a solution of 3,3′-bithiophene[31] (0.50 g; 3.0 mmol) in dry CS_2 (15 mL) and the solution was refluxed for 36 h. A saturated solution of $Na_2S_2O_5$ in water was added portionwise to the mixture until the brown color completely disappeared. The crude product, separated as a brown-colored solid, was repeatedly treated with hot ethanol to remove all soluble impurities (1.56 g; 80% yield; m.p. 180–183 °C); M.S. (E.I.$^+$) 640 *m/z*.

2,2′,4,4′,5,5′-Tetra(2-thienyl)-3,3′-bithiophene (T8$_3$): A mixture of hexabromo-3,3′-bithiophene (0.50 g, 0.8 mmol), 2-(tributylstannyl) thiophene (2.4 g, 6.4 mmol, Sigma–Aldrich) and 99% $Pd(PPh_3)_4$ (0.185 g, 1.6 mmol, Sigma–Aldrich) and *p*-xylene (25 mL), was refluxed under nitrogen atmosphere for 20 h. The reaction mixture was filtered on a silica gel cake (Merk 60, 230–70 mesh) to remove the catalyst, the solvent was removed under reduced pressure and the crude residue chromatographed on a silica gel column (Merk 60, 325–230 mesh) using a 4:1 mixture of *n*-hexane: CH_2Cl_2. Combined final fractions gave **T8$_3$** as a pale-yellow solid by removal of the solvent (0.15 g; 26% yield; m.p. = 120–125 °C (synt.)). ^{1}H NMR (400 MHz, $CDCl_3$) δ = 7.24 (2H, dd, J_1 = 5.1 Hz, J_2 = 1.2 Hz), 7.17 (2H, dd, J_1 = 5.1 Hz, J_2 = 1.1 Hz), 7.16 (2H, dd, J_1 = 5.1 Hz, J_2 = 1.0 Hz), 7.13 (2H, dd, J_1 = 3.7 Hz, J_2 = 1.1 Hz), 7.06 (2H, dd, J_1 = 3.7 Hz, J_2 = 1.1 Hz), 6.95 (2H, dd, J_1 = 5.1 Hz, J_2 = 3.7 Hz), 6.92 (2H, dd, J_1 = 5.1 Hz, J_2 = 3.7 Hz), 6.87 (2H, dd, J_1 = 5.1 Hz, J_2 = 3.5 Hz), 6.56 ppm (2H, dd, J_1 = 3.5 Hz, J_2 = 1.1 Hz); ^{13}C NMR (400 MHz, $CDCl_3$): δ = 135.7 (C), 135.6 (C), 135.0 (C), 134.9 (C), 133.3 (C), 132.6 (C), 131.9 (C), 128.9 (CH), 127.0 (CH), 126.9 (CH), 126.8 (CH), 126.6 (CH), 126.2 (CH), 126.1 (CH), 126.0 (CH), 125.1 (CH). MS (EI): 658 [M^+].

Theoretical Computations

Density Functional Theory calculations were performed with the atomic basis-set implementation available in Gaussian 09,[32] using the Pople's 6-31++G** basis-set and the long-range corrected hybrid B3LYP functional of Handy and co-workers (aka CAM-B3LYP)[33] for both structural and optical calculations.

Geometry optimizations were performed for the most reasonable isomers, and the transition state for enantiomer conversion of the most stable isomer was located with the three-structure STQN transition state searching method of Schlegel and co-workers.[34]

Optical calculations were of the linear-response Time-Dependent DFT type, and computed using the above functional in the adiabatic approximation, within the Casida's formulation of the problem of computing the longitudinal dielectric function. Calculations were performed both in vacuum and in the presence of a solvent reaction field. In the latter case, the Polarizable Continuum Model was adopted, using the solvent parameters appropriate for chloroform.[35]

Photophysical Characterization

Photophysical measurements were carried out in air-equilibrated toluene solutions at 298 K. Electronic absorption spectra were recorded on an Agilent Model 8543 spectrophotometer at room temperature and using quartz cells with 1.0 cm path length.

Steady-state emission spectra were obtained with an Edinburgh FLS980 spectrofluorometer equipped with a 450 W xenon arc lamp. Emission spectra are corrected for source intensity (lamp and grating) and emission spectral response (detector and grating) by standard correction curves.

Photoluminescence quantum yields (ϕ) were measured in optically dilute solution (typically 1.0×10^{-5} M) and compared to the quinine sulfate in 0.1 M H_2SO_4 solution at room temperature used as the standard reference emitter (ϕ = 0.58). All the ϕ values fall within a $\pm$5% range.[36]

Enantioselective HPLC

HPLC enantioseparations were performed by using the stainless-steel Chiralpak IB-3 and Chiralpak IB analytical (250 mm 4.6 mm i.d.) and semipreparative (250 mm L. × 10 mm i.d.) columns (Chiral Technologies Europe, Illkirch, France). All chemicals, solvents for HPLC, and syntheses and spectral grade solvents were purchased from Sigma–Aldrich and used without further purification.

The analytical HPLC apparatus consisted of a PerkinElmer 200 LC pump equipped with a Rheodyne injector, a 20 μL sample loop, a HPLC Dionex CC-100 oven and a Jasco Model CD 2095 Plus UV/CD detector. For semi-preparative separations, a PerkinElmer 200 LC pump equipped with a Rheodyne injector, a 500 μL sample loop, a PerkinElmer LC 101 oven and Waters 484 detector were used. The signal was acquired and processed by the Clarity software of DataApex.

Circular dichroism

The circular dichroism (CD) spectra of the (*S*)-(+)-**T8$_3$** and-(*R*)-(−)-**T8$_3$** were recorded by using a Jasco Model J-700 spectropolarimeter. The spectra were average-computed over three instrumental scans and the intensities are presented in terms of ellipticity values (mdeg).

Electrochemistry

Monomer characterization: Cyclic voltammetry (CV) experiments were performed using Autolab PGSTAT potentiostats of Eco-Chemie, controlled by a PC with the GPES software of the same manufacturer.

The voltammetric investigations on the **T8$_3$** redox features and oligomerization ability were carried out in traditional solvents acetonitrile (ACN, Sigma–Aldrich, anhydrous, $\geq$99.8%) and dichloromethane (CH_2Cl_2, Sigma–Aldrich) in both cases with 0.1 M tetrabutylammonium hexafluorophosphate as the supporting electrolyte (Fluka, $\geq$98%), or in ionic liquid 1-butyl-3-methylimidazolium hexafluorophosphate ((BMIM)PF_6, for catalysis, $\geq$98.5%, Fluka). A three-electrode V-shaped minicell (with 3 cm^3 of solution) was employed, including a glass-embedded glassy carbon disk (GC, Metrohm, S= 0.031 cm^2) or a gold disk (Au, Amel, S=0.033 cm^2) or platinum disk (Pt, Amel, S=0.031 cm^2) as the working electrode, a Pt disk or wire as the counter electrode, and an aqueous saturated calomel (SCE) as the operating reference electrode, inserted in a double bridge filled with the working medium, to avoid water and KCl leakage into the working solutions. The optimized preliminary polishing procedure for working disk electrodes consisted of treatment with a diamond powder of 1 μm diameter (Aldrich) on a wet DP-Nap cloth (Struers).

Oligomer film deposition and characterization: Depositions of conducting **T8$_3$** oligomer films by potentiodynamic electrooxidation were performed through 36 consecutive oxidative potential cycles at 0.2 $V s^{-1}$ around the first or the second oxidation peaks (with a monomer concentration of 0.5 mM), followed by repeated potential cycling in the same potential range in a monomer free solution; then the potential range was widened on the negative side, to look for charge trapping and other reduction processes. In the case of the (BMIM)PF_6 ionic liquid, depositions and film stability on SPEs were carried out at the 0.05 $mV s^{-1}$ potential scan rate with the monomer concentration of 12 mM.

Enantiorecognition tests: For the first enantioselection test, (*R*)- and (*S*)-conducting sensing oligomer films were electrodeposited from a drop (0.02–0.03 cm^3) of 12 mM (*S*)- and (*R*)-**T8$_3$** monomer solutions, dispensed on screen-printed gold working electrodes (Au-SPEs, Metrohm, 61208210) by 36 consecutive oxidative CV cycles at 0.05 $V s^{-1}$ scan rate, followed by several potential cycles in a monomer-free blank medium. The voltammetric characteristics of (*R*)- and (*S*)-*N*,*N*-dimethyl-1-ferrocenylethylamine probes (Sigma–Aldrich, $\geq$97%) were then recorded, both enantiopure and in 1:1 ratio, dissolved in a drop of (BMIM)PF_6 at 0.18 mM concentration.

The second enantioselection test was carried out on the (*R*)- and (*S*)-**T8$_3$** oligomer films deposited by electropolymerization on Au SPEs from (BMIM)PF_6 as described above, testing 0.16 mM aqueous hydrogen chloride solutions of L- and D-DOPA ((*S*)- and (*R*)-3,4-dihydroxy-phenylalanine, respectively, Sigma–Aldrich, $\geq$98%, 0.05 M).

MIP Experimental

Instrumentation: An SP-300 Modular Research Grade Potentiostat/Galvanostat/FRA of Bio-Logic, controlled by the EC-lab software of the same manufacturer was used for deposition of the molecularly imprinted with TATAAA (T=thymine, A=adenine) polymer (MIP-TATAAA) film on the 21 mm^2 Au film coated glass slide working electrode. An Ag/AgCl and Pt grid served as the reference and counter electrode, respectively.

For measurements using an extended-gate field effect transistor (EG-FET), a Keithley 2636B dual-channel source meter (1 fA, 10 A pulse) was employed. An MIP-TATAAA film coated Au-glass slide electrode, connected to a CD4007UB MOSFET, was used as the extended gate while a Pt grid served as the pseudo-reference electrode. An optimized low gate voltage of 1.50 V was applied by polarization of the extended-gate electrode against the pseudo-reference electrode.

Chemosensor preparation: The MIP-TATAAA film was deposited on the Au-glass electrode by potentiodynamic electropolymerization from the 40 μM TATAAA, 0.1 mM 4-[bis(2,2′-bithien-5-yl)methane]phenyl thymine-1-acetic acid ester (functional monomer **4**), 0.05 mM 4-[bis(2,2′-bithien-5-yl]methane] phenyl 2-adenine ethyl ether (functional monomer **5**), 0.2 mM 2,2′,4,4′,5,5′-tetra(2-thienyl)-3,3′-bithiophene **T8$_3$** (cross-linking monomer), and 0.1 M (TBA)ClO_4 (supporting electrolyte) solution of the volume ratio of acetonitrile-to-water-to-toluene-to-isopropanol equal to 7.5:1:1:0.5. For this deposition, the potential was scanned from 0.5 to 1.25 V at the rate of 50 $mV s^{-1}$ for six current-potential cycles, which resulted in deposition of the MIP-TATAAA film. Then, the TATAAA template was extracted from this film with 0.1 M NaOH for 45 min at room temperature. In the same manner, a control non-imprinted polymer (NIP) film was prepared in the absence of the TATAAA template in the solution for the electropolymerization. The TATAAA-extracted MIP and NIP films served as recognition units of the EG-FET chemosensors.

Acknowledgements

The financial support of Fondazione Cariplo (grants 2011-0417 and 2011-1851) is gratefully acknowledged. The research on inherently chiral materials and surfaces is developed in the context of the SmartMatLab Centre project, cofunded by Regione Lombardia (EU FESR and FSE funds), Fondazione Cariplo, Università degli Studi di Milano and ISTM-CNR. Laboratori Alchemia s.r.l is acknowledged for supporting the cover cost.

Keywords: chirality · enantiorecognition · hyperbranching · molecularly imprinted polymers · oligothiophenes

[1] F. Sannicolò, S. Arnaboldi, T. Benincori, V. Bonometti, R. Cirilli, L. Dunsch, W. Kutner, G. Longhi, P. R. Mussini, M. Panigati, M. Pierini, S. Rizzo, *Angew. Chem. Int. Ed.* **2014**, *53*, 2623–2627; *Angew. Chem.* **2014**, *126*, 2661–2665.

[2] F. Sannicolò, P. R. Mussini, T. Benincori, R. Cirilli, S. Abbate, S. Arnaboldi, S. Casolo, E. Castiglioni, G. Longhi, R. Martinazzo, M. Panigati, M. Pappini, E. Quartapelle Procopio, S. Rizzo, *Chem. Eur. J.* **2014**, *20*, 15298–15302.

[3] For a review on chiral conducting polymers, see a) L. A. P. Kane-Maguire, G. G. Wallace, *Chem. Soc. Rev.* **2010**, *39*, 2545–2576and references therein; b) B. M. W. Langeveld-Voss, M. P. T. Christiaans, R. A. J. Janssen, E. W. Meijer, *Macromolecules* **1998**, *31*, 6702–67704; c) M. Schwientek, S. Pleus, C. H. Hamann, *J. Electroanal. Chem.* **1999**, *461*, 94–101; d) B. M. W. Langeveld-Voss, R. J. M. Waterval, R. A. J. Janssen, E. W. Meijer, *Macromolecules* **1999**, *32*, 227–230; e) B. M. W. Langeveld-Voss, R. A. J. Janssen, E. W. Meijer, *J. Mol. Struct.* **2000**, *521*, 285–301; f) B. J. De Lacy Costello, N. M. Ratcliffe, P. S. Sivanand, *Synth. Met.* **2003**, *139*, 43–55; g) T. Verbiest, S. Sioncke, G. Koeckelberghs, C. Samin, A. Persoons, E. Botek, JM. André, B. Campagne, *Chem. Phys. Lett.* **2005**, *404*, 112–115; h) H. Goto, Y. S. Yeong, K. Akagi, *Macromol. Rapid Commun.* **2005**, *26*, 164–167; i) A. S. Ribeiro, L. M. O. Ribeiro, S. M. M. Leite, J. Da Silva Jr., J. C. Ramos, M. Navarro, J. Tonholo, *Polymer* **2006**, *47*, 8430–8435; j) L. Torsi, G. M. Farinola, F. Marinelli, M. C. Tanese, O. H. Omar, L. Valli, F. Babudri, F. Palmisano, P. G. Zambonin, F. Naso, *Nat. Mater.* **2008**, *7*, 412–417; k) D. Cornelis, E. Franz, I. Asselberghs, K. Clays, T. Verbiest, G. Koeckelberghs, *J. Am. Chem. Soc.* **2011**, *133*, 1317–1327.

[4] M. Lemaire, D. Delabouglise, R. Garreau, A. Guy, J. Roncali, *J. Chem. Soc. Chem. Commun.* **1988**, 658–661.

[5] S. Arnaboldi, T. Benincori, R. Cirilli, W. Kutner, P. R. Mussini, F. Sannicolò, *Chem. Sci.* **2015**, *6*, 1706–1711.

[6] T. Benincori, V. Bonometti, F. De Angelis, L. Falciola, M. Muccini, P. R. Mussini, T. Pilati, G. Rampinini, S. Rizzo, S. Toffanin, F. Sannicolò, *Chem. Eur. J.* **2010**, *16*, 9086 – 9098.
[7] T. Benincori, M. Capaccio, F. De Angelis, L. Falciola, M. Muccini, P. R. Mussini, A. Ponti, S. Toffanin, P. Traldi, F. Sannicolò, *Chem. Eur. J.* **2008**, *14*, 459 – 471.
[8] a) C. J. Xia, X. W. Fan, J. Locklin, R. C. Advincula, *Org. Lett.* **2002**, *4*, 2067 – 2070; b) C. Q. Ma, E. Mena-Osteriz, T. Debardemaeker, M. M. Wienk, R. A. J. Janssen, P. Bäuerle, *Angew. Chem. Int. Ed.* **2007**, *46*, 1679 – 1713; *Angew. Chem.* **2007**, *119*, 1709 – 1713; c) S. Karpe, A. Cravino, P. Frère, M. Allain, G. Mabon, J. Roncali, *Adv. Funct. Mater.* **2007**, *17*, 1163 – 1171; d) C. Q. Ma, M. Fondrona, M. C. Schikora, M. M. Wienk, R. A. Janssen, P. Bäuerle, *Adv. Funct. Mater.* **2008**, *18*, 3323 – 3331; e) T. V. Richter, S. Link, R. Hanselmann, S. Ludwigs, *Macromol. Rapid Commun.* **2009**, *30*, 1323 – 1327; f) T. V. Richter, C. Bühler, S. Ludwigs, *J. Am. Chem. Soc.* **2012**, *134*, 43 – 46; g) T. V. Richter, C. H. Braun, S. Link, M. Scheuble, E. J. W. Crossland, F. Stelzl, U. Würfel, S. Ludwigs, *Macromolecules* **2012**, *45*, 5782 – 5788.
[9] A. Bilge, A. Zen, M. Forster, H. Li, F. Galbrecht, B. S. Nehls, T. Farrell, D. Neher, U. Scherf, *J. Mater. Chem.* **2006**, *16*, 3177 – 3182.
[10] A. Zen, P. Pingel, D. Neher, U. Scherf, *Phys. Status Solidi A* **2008**, *205*, 440 – 448.
[11] S. Becker, J. Seixas de Melo, A. L. Maçanita, F. Elisei, *J. Phys. Chem.* **1996**, *100*, 18683 – 18695.
[12] P. A. Chaloner, S. R. Gunatunga, P. B. Hitchcock, *J. Chem. Soc. Perkin Trans. 2* **1997**, 1597 – 1604.
[13] A. Facchetti, M.-H. Yoon, C. L. Stern, G. R. Hutchison, M. A. Ratner, T. J. Marks, *J. Am. Chem. Soc.* **2004**, *126*, 13480 – 13501.
[14] R. Meerholz, J. Heinze, *Electrochim. Acta* **1996**, *41*, 1839 – 1854.
[15] J. Heinze, *Top. Curr. Chem.* **1990**, *152*, 1 – 47.
[16] C. Reichardt, *Solvent Effects in Organic Chemistry*, 2nd Ed., Wiley-VCH, Weinheim, **1990**.
[17] A. Pietrzyk, S. Suriyanarayanan, W. Kutner, R. Chitta, M. E. Zandler, F. D'Souza, *Biosens. Bioelectron.* **2010**, *25*, 2522 – 2529.
[18] T. Huynh, A. Wojnarowicz, M. Sosnowska, S. Srebrnik, T. Benincori, F. Sannicolò, F. D'Souza, W. Kutner, *Biosens. Bioelectron.* **2015**, *70*, 153 – 160.
[19] F. Svedberg, Y. Alaverdyan, P. Johansson, M. Käll, *J. Phys. Chem. B* **2006**, *110*, 25671 – 25677.
[20] L. A. Song, D. D. Shan, M. W. Zhao, B. A. Pink, K. A. Minnehan, L. York, M. Gardel, S. Sullivan, A. F. Phillips, R. B. Hayman, D. R. Walt, D. C. Duffy, *Anal. Chem.* **2013**, *85*, 1932 – 1939.
[21] G. J. Tsongalis, L. M. Silverman, *Clin. Chim. Acta* **2006**, *369*, 188 – 192.
[22] S. M. McQuaig, T. M. Scott, J. O. Lukasik, J. H. Paul, V. J. Harwood, *Appl. Environ. Microbiol.* **2009**, *75*, 3379 – 3388.
[23] D. R. Christensen, L. J. Hartman, B. M. Loveless, M. S. Frye, M. A. Shipley, D. L. Bridge, M. J. Richards, R. S. Kaplan, J. Garrison, C. D. Baldwin, D. A. Kulesh, D. A. Norwood, *Clin. Chem.* **2006**, *52*, 141 – 145.
[24] F. Postollec, H. Falentin, S. Pavan, J. Combrisson, D. Sohier, *Food Microbiol.* **2011**, *28*, 848 – 861.
[25] P. Bergveld, *IEEE Trans. Biomed. Eng.* **1970**, *17*, 70 – 71.
[26] C.-P. Chen, A. Ganguly, C.-U. Lu, T.-Y. Chen, C.-C. Kuo, R.-S. Chen, W.-H. Tu, W. B. Fischer, K.-H. Chen, L.-C. Chen, *Anal. Chem.* **2011**, *83*, 1938 – 1943.
[27] Z. Iskierko, M. Sosnowska, P. S. Sharma, T. Benincori, F. D'Souza, I. Kaminska, K. Fronc, K. Noworyta, *Biosens. Bioelectron.* **2015**, *74*, 526 – 533.
[28] M. Dabrowski, P. S. Sharma, Z. Iskierko, K. Noworyta, M. Cieplak, W. Lisowski, S. Oborska, A. Kuhn, W. Kutner, *Biosens. Bioelectron.* **2016**, *79*, 627 – 635.
[29] P. S. Sharma, Z. Iskierko, A. Pietrzyk-Le, F. D'Souza, W. Kutner, *Electrochem. Comm.* **2015**, *50*, 81 – 87.
[30] U. Dahlmann, R. Neidleinn, *Helv. Chim. Acta* **1996**, *79*, 755 – 766.
[31] R. Satapathy, Y. H. Wu, H. C. Lin, *Org. Lett.* **2012**, *14*, 2564 – 2567.
[32] Gaussian 09, Revision A.02, M. J. Frisch, G. W. Trucks, H. B. Schlegel, G. E. Scuseria, M. A. Robb, J. R. Cheeseman, G. Scalmani, V. Barone, B. Mennucci, G. A. Petersson, H. Nakatsuji, M. Caricato, X. Li, H. P. Hratchian, A. F. Izmaylov, J. Bloino, G. Zheng, J. L. Sonnenberg, M. Hada, M. Ehara, K. Toyota, R. Fukuda, J. Hasegawa, M. Ishida, T. Nakajima, Y. Honda, O. Kitao, H. Nakai, T. Vreven, J. A. Montgomery, Jr., J. E. Peralta, F. Ogliaro, M. Bearpark, J. J. Heyd, E. Brothers, K. N. Kudin, V. N. Staroverov, T. Keith, R. Kobayashi, J. Normand, K. Raghavachari, A. Rendell, J. C. Burant, S. S. Iyengar, J. Tomasi, M. Cossi, N. Rega, J. M. Millam, M. Klene, J. E. Knox, J. B. Cross, V. Bakken, C. Adamo, J. Jaramillo, R. Gomperts, R. E. Stratmann, O. Yazyev, A. J. Austin, R. Cammi, C. Pomelli, J. W. Ochterski, R. L. Martin, K. Morokuma, V. G. Zakrzewski, G. A. Voth, P. Salvador, J. J. Dannenberg, S. Dapprich, A. D. Daniels, O. Farkas, J. B. Foresman, J. V. Ortiz, J. Cioslowski, D. J. Fox, Gaussian, Inc., Wallingford CT, **2009**.
[33] T. Yanai, D. P. Tew, N. C. Handy, *Chem. Phys. Lett.* **2004**, *393*, 51 – 57.
[34] a) C. Peng, H. B. Schlegel, *Israel J. Chem.* **1993**, *33*, 449 – 454; b) C. Peng, P. Y. Ayala, H. B. Schlegel, M. J. Frisch, *J. Comput. Chem.* **1996**, *17*, 49 – 56.
[35] M. Cossi, N. Rega, G. Scalmani, V. Barone, *J. Comput. Chem.* **2003**, *24*, 669 – 681.
[36] J. R. Lakowicz, *Principles of Fluorescence Spectroscopy*, 3rd Ed. Springer, New York, **2006**.

Received: December 4, 2015
Published online on June 20, 2016